Raman scattering from crystals of the diamond structure

R.A. Cowley

RAMAN SCATTERING FROM CRYSTALS OF THE DIAMOND STRUCTURE

By R. A. COWLEY,
Chalk River Nuclear Laboratories, Chalk River, Ontario, Canada.

Résumé. — On discute la théorie de la diffusion Raman de la lumière par des cristaux du type diamant, et on effectue les calculs détaillés pour la diffusion par le germanium, le silicium et le diamant. L'anharmonicité entre les modes normaux de vibration produit un élargissement de la raie à un phonon. La forme de cette raie dépend du comportement détaillé de la durée de vie et de la fréquence du mode optique de grande longueur d'onde. L'anharmonicité amène aussi un couplage entre les diffusions à un et à deux phonons, qui tend, en partie, à écarter le centre de la raie à un phonon de la fréquence du mode optique.

Les modèles en coquille adaptés aux courbes de dispersion mesurées servent au calcul des modes normaux de vibration. Les éléments des matrices à un et à deux phonons de la diffusion Raman sont évalués au moyen de la méthode du modèle en coquille, appliquée à ces modèles particuliers, et les spectres sont calculés, en tenant compte des effets de l'anharmonicité de la diffusion, par un phonon. La comparaison des résultats avec les données expérimentales connues montre que les détails du spectre dépendent considérablement de la polarisation de la lumière et de l'orientation du cristal.

Abstract. — The theory of the Raman scattering of light from crystals of the diamond structure is discussed and detailed calculations made of the scattering by germanium, silicon and diamond. The anharmonicity between the normal modes of vibrations gives rise to a broadening of the one-phonon peak. The shape of this peak then depends upon the detailed behaviour of the lifetime and frequency of the long wavelength optic mode. The anharmonicity also introduces a coupling between the one and two-phonon scattering, part of which tends to shift the center of the one phonon Raman peak away from the frequency of the optic mode. Shell models which were fitted to the measured dispersion curves are used to calculate the frequencies of the normal modes of vibration. The one and two-phonon matrix elements for the Raman scattering are evaluated by means of the shell model formalism for these models and the spectra calculated including the effects of anharmonicity on the one phonon scattering. The results which are compared with the available experimental results show that the details of the spectra depend considerably on the polarization of the light and on the orientation of the crystal.

1. **Introduction.** — The theory of the Raman scattering of light by the lattice vibrations of a crystal shows that it depends on the way in which the lattice vibrations modify the electronic polarizability, $P_{\alpha\beta}$, of the crystal as described by Born and Huang [1], and by Loudon [2].

The intensity of the scattered light depends upon the polarizations of the light and upon the crystal orientation. If the electric vector of the incident light is defined by **E**, and the polarization of the electric vector of the scattered light by **n**, the intensity of scattering per unit solid angle is [1]

$$I = \frac{\omega_0^4}{2\pi c^3} \sum_{\alpha\beta\gamma\delta} n_\alpha n_\gamma I_{\alpha\beta\gamma\delta} E_\beta E_\delta, \qquad (1.1)$$

where

$$I_{\alpha\beta\gamma\delta} = \sum_{\nu'} < \nu|P^*_{\alpha\beta}|\nu' > < \nu'|P_{\gamma\delta}|\nu > \delta\left(\Omega - \frac{\varepsilon_\nu - \varepsilon_{\nu'}}{\hbar}\right). \qquad (1.2)$$

The frequency of the incident light is ω_0, ν is the initial state of the crystal of energy ε_ν, ν' the final state of energy $\varepsilon_{\nu'}$, and Ω the change in frequency of the light. The expression (1.2) is most readily evaluated by the use of the techniques of many body theory (for example Abrikosov, Gorkov and Dyzaloshinski [3]). The Fourier transform of the thermodynamic time ordered Green's functions $G(P^*_{\alpha\gamma} P_{\beta\delta}, \Omega)$ are easily evaluated by the use of these techniques, and

$$I_{\alpha\beta\gamma\delta} = \{\exp(\beta\hbar\Omega) - 1\}^{-1} \lim_{\varepsilon \to 0^+} \{ G(P^*_{\alpha\beta} P_{\gamma\delta}, \Omega + i\varepsilon) - G(P^*_{\alpha\beta} P_{\gamma\delta}, \Omega - i\varepsilon) \}. \qquad (1.3)$$

The Raman scattering is now obtained by expanding the polarizability of the crystal as a power series and evaluating the Green's functions by means of diagrams [4]. In each diagram the phonons associated with the $P^*_{\alpha\beta}$ operator enter on the left, while those associated with $P_{\gamma\delta}$ leave on the right. In between they interact with one another through the anharmonic interactions in the crystal. The rules for calculating the contributions of these diagrams have been given by Maradudin and Fein [5] and by Cowley [6].

The Raman spectra of the crystal can then be obtained from the $I_{\alpha\beta\gamma\delta}$, appropriate for the particular conditions of the experiment. The spectra are dependent upon the state of polarization of both the incident and scattered light, and also on

the crystal orientation. A table of the appropriate combinations of the $I_{\alpha\beta\gamma\delta}$ for some typical experiments is given in [4].

Two difficulties arise in the detailed calculation of the Raman spectra. Firstly the frequencies and eigenvectors of the normal modes of vibration are usually unknown. In this paper this difficulty is overcome by the use of models whose parameters were fitted to give good agreement with measurements of the dispersion curves, as made by inelastic neutron scattering techniques. The models are described in detail by Dolling [7] and by Dolling and Cowley [8].

The second difficulty arises because the influence of the lattice vibrations on the polarizability of the crystal is unknown. These calculations are performed by assuming that the interaction is of a very simple form between nearest neighbour ions, as described in the next section. The detailed form of the Raman spectra of the diamond structure materials depends on the behaviour of the one-phonon contribution. This is largely influenced by the anharmonic interactions of the long wavelength optic mode of vibration with the other normal modes. These interactions have been calculated by means of the parameters of the anharmonicity determined from the experimental thermal expansion of the crystal [8].

In section 3 the detailed expressions for the Raman spectra are given, including the effects of anharmonicity on the long wavelength optic mode. The calculation of the spectra and the results are described in section 4.

Measurements of the Raman spectra are frequently used to deduce critical point frequencies (Loudon [2] and Bilz, Geick and Renk [9]). Some of the difficulties in deciding and interpreting these critical point frequencies are described in section 5. The results are summarized and discussed in section 6.

2. **The polarizability.** — The electronic polarizability of a crystal may be expanded as a power series in the phonon coordinates [1] :

$$P_{\alpha\beta} = P^{(0)}_{\alpha\beta} + \sum_j P_{\alpha\beta}(\mathbf{0}j)\, A(\mathbf{0}j) + \sum_{\mathbf{q}jj'} P_{\alpha\beta}(\mathbf{q}jj')\, A(-\mathbf{q}j)\, A(\mathbf{q}j') + \ldots, \quad (2.1)$$

where the $A(\mathbf{q}j)$ are the sum of the phonon creation and destruction operators. The one-phonon contribution arises from the long wavelength optic mode of vibration in the diamond structure, the symmetry of which shows that $P_{\alpha\beta}(\mathbf{0}j)$ is non-zero only if α and β are unequal [2]. The coefficients of the two-phonon term, $P_{\alpha\beta}(\mathbf{q}jj')$, are more complicated and depend both on the wave vector $\mathbf{q}$ and the indices j and j' of the normal modes. Birman [10], Johnson and Loudon [11] and Kleinman [12] have given the selection rules for these coefficients which result from the symmetry of the normal modes.

In these calculations the coefficients are determined by assuming a form for the interaction between the ions giving rise to the polarizability. The two-phonon contribution to the polarizability may be written as

$$\sum_{\gamma\delta} \sum_{\substack{ll' \\ \varkappa\varkappa'}} P_{\alpha\beta,\gamma\delta} \begin{pmatrix} l & l' \\ \varkappa & \varkappa' \end{pmatrix} U_\gamma(l\varkappa)\, U_\delta(l'\varkappa'), \quad (2.2)$$

where $\mathbf{u}(l\varkappa)$ is the displacement of the $\varkappa^{th}$ ion in the l^{th} unit cell. The number of arbitrary coefficients needed to describe the interactions in equation (2.2) is restricted by the symmetry of the crystal and by making physical approximations about the form of the interaction. In these calculations the simplest form of one parameter nearest neighbour interaction has been used in which

$$P_{\alpha\beta,\gamma\delta} \begin{pmatrix} l & l' \\ \varkappa & \varkappa' \end{pmatrix} = X R_\alpha R_\beta R_\gamma R_\delta, \quad (2.3)$$

where X is a constant and $\mathbf{R}$ is the vector distance of the ion $(l'\varkappa')$ from the ion $(l\varkappa)$ and the interaction is restricted to nearest neighbours. The expressions for $(l'\varkappa') = (l\varkappa)$ were deduced by the use of translational invariance. The coefficients of the two-phonon term in equation (2.1) are then given by

$$P_{\alpha\beta}(\mathbf{q}jj') = \frac{X'}{N} (\omega(\mathbf{q}j)\, \omega(\mathbf{q}j'))^{-1/2} \sum_{\gamma\delta} \sum_{\substack{ll' \\ \varkappa\varkappa'}} P_{\alpha\beta,\gamma\delta} \begin{pmatrix} l & l' \\ \varkappa & \varkappa' \end{pmatrix} e^*_\gamma(\varkappa, \mathbf{q}j)\, e_\delta(\varkappa', \mathbf{q}j') \exp(i\mathbf{q}.\mathbf{R}). \quad (2.4)$$

The eigenvectors of the normal modes are written $\mathbf{e}(\varkappa, \mathbf{q}j)$ and the frequencies $\omega(\mathbf{q}j)$ while X' is another constant.

This development of detailed expressions for the two-phonon contribution to equation (2.1) may be compared with those deduced earlier [4] by use of the shell model formalism. Equation (9) of [4] is very similar to equation (2.4) if the terms depending on the displacements of the shells are neglected. The one parameter interaction we have used here is equivalent to assuming that the interaction in equation (10) of [4] is a central force in which the fourth derivative terms are by far the largest. The parameters for the calculation of the Raman spectra of the alkali halides were deduced earlier by assuming that all the short range interaction acts through the shells. In the case of the diamond structure this approximation necessarily gives rise to no Raman scattering, when translational invariance is applied to the interaction. The parameter of the two-phonon Raman scattering in the diamond structure could not there-

fore readily be deduced from other measurements.

The contributions included by the expressions (2.3) and (2.4) are therefore very similar to those of equations (9) and (10) of [4]. However the shell model formalism shows that there is an additional contribution to the two-phonon scattering from two optic modes of long wavelength. Such a scattering is observed experimentally in diamond [13] and it is necessary to add in this extra two-phonon term to explain the magnitude of this scattering.

3. **The Raman spectra.** — The Raman spectra can be obtained from the expressions given in I and the expansion for the polarizability (2.1). The detailed shape of the one-phonon spectra is determined by the anharmonic interactions involving the optic mode of vibration. The extra contribution to the Hamiltonian from the anharmonic interactions is written as

$$H_A = \sum_{\substack{q_1 q_2 q_3 \\ j_1 j_2 j_3}} V\begin{pmatrix} q_1 & q_2 & q_3 \\ j_1 & j_2 & j_3 \end{pmatrix} A(q_1 j_1)\, A(q_2 j_2)\, A(q_3 j_3) + \cdots \tag{3.1}$$

The anharmonic interactions alter the self-energies of the normal modes. The three lowest order diagrams are shown in figure 1, and their effect on

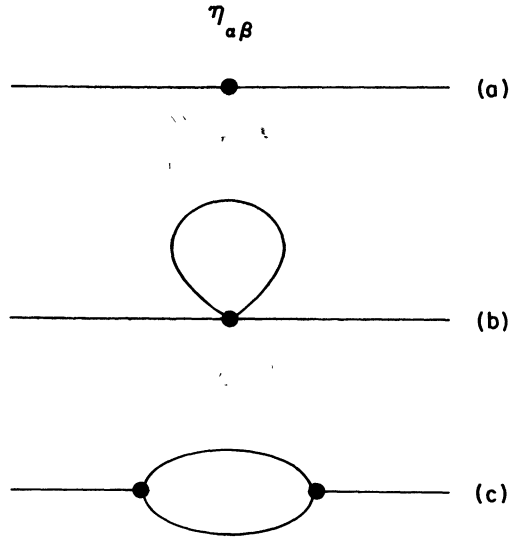

FIG. 1. — The three lowest order diagrams which contribute to the self-energy of the normal modes. Diagram (a) arises from the thermal expansion while the other diagrams arise from the interactions between the normal modes.

the optic mode of vibration is to make its frequency and lifetime dependent upon both the temperature and the applied frequency (Ω) :

$$\omega^2(oj, \Omega) = \omega^2(oj) + 2\omega(oj)\,[\Delta(oj, \Omega) + i\Gamma(oj, \Omega)]. \tag{3.2}$$

The detailed expressions for the contributions to $\Delta(oj, \Omega)$ and $\Gamma(oj, \Omega)$, shown in figure 1, are [5],

$$\Delta(oj, \Omega) = 2\sum_{\alpha\beta} V_{\alpha\beta}\begin{pmatrix} o & o \\ j & j \end{pmatrix} U^T_{\alpha\beta} + \frac{12}{\hbar}\sum_{qj'} V\begin{pmatrix} o & o & q & -q \\ j & j & j' & j' \end{pmatrix}(2n(qj') + 1) - \frac{18}{\hbar^2}\sum_{qj_1j_2}\left| V\begin{pmatrix} o & q & -q \\ j & j_1 & j_2 \end{pmatrix}\right|^2 R(\Omega). \tag{3.3}$$

Diagram (*a*), figure 1, and the first term of this equation arise from the thermal expansion of the crystal, while the second term is from diagram (*b*). The function $R(\Omega)$ is

$$\frac{n(qj_1) + n(qj_2) + 1}{(\Omega + \omega(qj_1) + \omega(qj_2))_p} + \frac{n(qj_1) + n(qj_2) + 1}{(\omega(qj_1) + \omega(qj_2) - \Omega)_p} + \frac{n(qj_2) - n(qj_1)}{(\omega(qj_1) - \omega(qj_2) - \Omega)_p} + \frac{n(qj_1) - n(qj_2)}{(\omega(qj_2) - \omega(qj_1) - \Omega)_p}. \tag{3.4}$$

The occupation number of the normal mode is $n(qj)$ and its inverse lifetime

$$\Gamma(oj, \Omega) = \frac{18}{\hbar^2}\sum_{qj_1j_2}\left| V\begin{pmatrix} o & q & -q \\ j & j_1 & j_2 \end{pmatrix}\right|^2 S(\Omega), \tag{3.5}$$

where

$$S(\Omega) = -\pi(n(qj_1) + n(qj_2) + 1)\,[\delta(\omega(qj_1) + \omega(qj_2) + \Omega) - \delta(\Omega - \omega(qj_1) - \omega(qj_2))] + \pi(n(qj_1) - n(qj_2))\,[\delta(\omega(qj_1) - \omega(qj_2) + \Omega) - \delta(\Omega - \omega(qj_1) + \omega(qj_2))]. \tag{3.6}$$

The diagrams which contribute to the Raman spectra are shown in figure 2. The one-phonon contribution to I_{XYXY} is

$$\frac{2}{\pi}\{\exp(\beta\hbar\Omega) - 1\}^{-1} \frac{P^*_{XY}(oj)\, P_{XY}(oj)\, \Gamma(oj, \Omega)\, \omega(oj)^2}{\{\omega(oj)^2 + 2\omega(oj)\Delta(oj, \Omega) - \Omega^2\}^2 + 4\omega(oj)^2\Gamma(oj, \Omega)^2}. \tag{3.7}$$

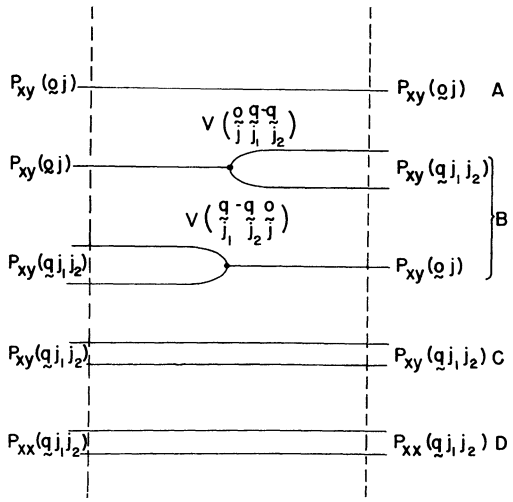

FIG. 2. — The lowest order diagrams which contribute to the Raman spectra of the diamond structure materials.

Diagrams (*b*) also contribute only to I_{XYXY}, and involves both one and two-phonon processes :

$$-\frac{6}{\pi}\{\exp(\beta\hbar\Omega)-1\}^{-1}\sum_{\mathbf{q}j_1j_2}P^*_{XY}(\mathbf{0}j)\,V\begin{pmatrix}\mathbf{0} & -\mathbf{q} & \mathbf{q}\\ j & j_1 & j_2\end{pmatrix}P_{XY}(\mathbf{q}j_1j_2)$$
$$\left[\frac{4\omega(\mathbf{0}j))^2\,\Gamma(\mathbf{0}j,\,\Omega)\,R(\Omega)+2\omega(\mathbf{0}j)\,(\omega(\mathbf{0}j))^2+2\omega(\mathbf{0}j)\,\Delta(\mathbf{0}j,\,\Omega)-\Omega^2)\,S(\Omega)}{(\omega(\mathbf{0}j))^2+2\omega(\mathbf{0}j))\,\Delta(\mathbf{0}j,\,\Omega)-\Omega^2)^2+4\omega(\mathbf{0}j))^2\,\Gamma(\mathbf{0}j,\,\Omega)^2}\right]. \quad (3.8)$$

Diagrams (*c*) and (*d*) are the two-phonon contributions to I_{AYXY} and I_{XXXX} respectively ; diagram (*d*) gives

$$\frac{2}{\pi}\{\exp(\beta\hbar\Omega)-1\}^{-1}$$
$$\sum_{\mathbf{q}j_1j_2}P^*_{XX}(\mathbf{q}j_1j_2)\,P_{XX}(\mathbf{q}j_2j_1)\,S(\Omega). \quad (3.9)$$

The Raman spectra can now be obtained in detail by the use of these equations and those for the coefficients in the expansion of the polarizability (2.1).

4. **Calculations and results.** — The one-phonon scattering cross-section depends in detail on the anharmonic interaction of the long wavelength optic mode with the other normal modes. The calculation of the shift, $\Delta(\mathbf{0}j,\,\Omega)$, and inverse lifetime, $\Gamma(\mathbf{0}j,\,\Omega)$, have been performed using the eigenvectors and frequencies of harmonic models, obtained by fitting the parameters of the models to give excellent agreement with the dispersion curves as measured by inelastic neutron scattering. The models are described in detail by Dolling [7] and by Dolling and Cowley [8].

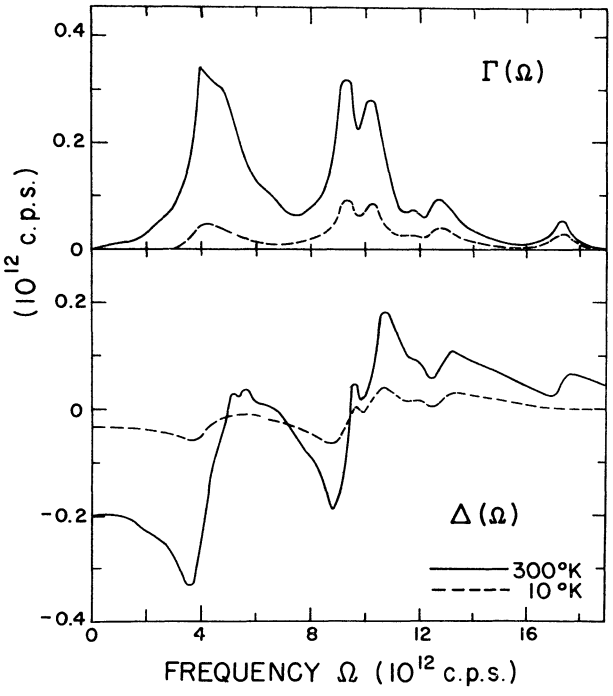

FIG. 3. — The shift in frequency, $\Delta(\mathbf{0}j,\,\Omega)$, and the inverse lifetime, $\Gamma(\mathbf{0}j,\,\Omega)$, as a function of the applied frequency, Ω, for the optic mode of germanium at 10 °K and 300 °K.

The anharmonic interactions $V\begin{pmatrix}\mathbf{0} & \mathbf{q} & -\mathbf{q}\\ j & j_1 & j_2\end{pmatrix}$ were deduced by assuming they were two body central forces between nearest neighbours, and finding the parameters which give best agreement with the experimentally measured thermal expansion as described by Dolling and Cowley [8]. The calculation of the third contribution, diagram (*c*) of figure 1, to $\Delta(\mathbf{0}j,\,\Omega)$ and to $\Gamma(\mathbf{0}j,\,\Omega)$ were then performed numerically by sampling $\mathbf{q}$ over 4 000 wave vectors in the full Brillouin zone. The results for germanium at 10 °K and 300 °K are shown in figure 3 as a function of the applied frequency. The contributions to the shift from diagrams (*a*) and (*b*) of figure 1 were not evaluated because they do not alter with applied frequency, and furthermore in calculations for the alkali halides they almost exactly cancel [6]. It is of interest that both the shift and inverse lifetime are quite strongly dependent upon the applied frequency, Ω. In any particular experiment the inverse lifetime is normally taken as given by the width of the one-phonon peak. This is roughly approximated by $\Gamma(\mathbf{0}j,\,\omega(\mathbf{0}j))$ and the shift in frequency by $\Delta(\mathbf{0}j,\,\omega(\mathbf{0}j))$. These are listed in the table at various temperatures for germanium, silicon and diamond.

TABLE

THE SHIFT IN FREQUENCY $\Delta(\mathbf{0}j,\,\omega(\mathbf{0}j))$ AND THE INVERSE LIFETIME $\Gamma(\mathbf{0}j,\,\omega(\mathbf{0}j))$ OF THE OPTIC MODES, FOR DIAGRAM (c) OF FIGURE 1. UNITS 10^{12} c. p. s.

TEMPERATURE °K	$\Delta(\mathbf{0}j,\,\omega(\mathbf{0}j))$	$\Gamma(\mathbf{0}j,\,\omega(\mathbf{0}j))$
Diamond	$\omega(\mathbf{0}j) = 39.95$	
10	— 0.098	0.041
300	— 0.099	0.045
500	— 0.108	0.056
1 000	— 0.154	0.094
Silicon	$\omega(\mathbf{0}j) = 15.54$	
10	— 0.12	0.17
100	— 0.15	0.18
300	— 0.26	0.29
500	— 0.39	0.38
Germanium	$\omega(\mathbf{0}j) = 9.01$	
10	— 0.05	0.08
100	— 0.07	0.12
300	— 018	0.25
500	— 0.31	0.37

Once the form of $\Delta(0j, \Omega)$ and $\Gamma(0j, \Omega)$ have been calculated the shape of the one-phonon peak is given by equation (3.7). The results for germanium are shown in figure 4, and for silicon in figure 5 by the curves A and AA. Curve AA shows the fine structure resulting from the frequency dependence of $\Delta(0j, \Omega)$ and $\Gamma(0j, \Omega)$ while A shows the principal peak. Since the numerical value of $P_{\alpha\beta}(0j)$ is unknown the intensity scale is arbitrary.

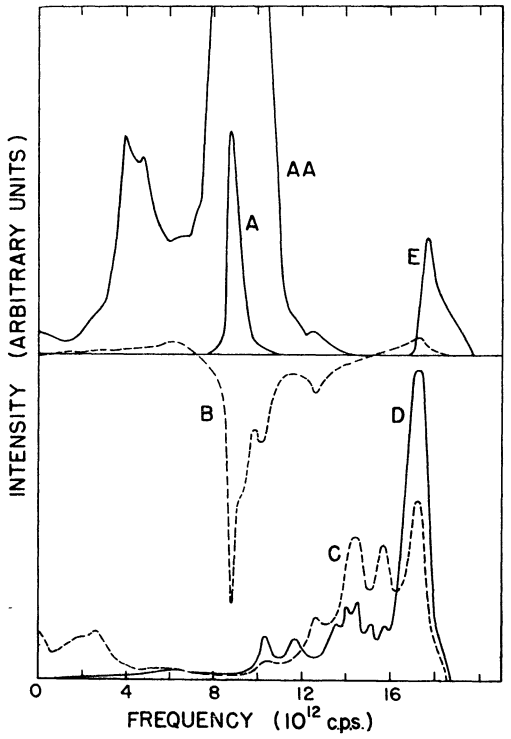

FIG. 4. — The contributions to the Raman spectra of germanium at 300 °K. Curves AA and A show the one-phonon part. Curve AA is on 100 times larger scale than A. B arises from the joint one-and two-phonon type of process, C is the two-phonon I_{XYXY} contribution, and D the I_{XXXX} contribution. E results from the two phonon contribution from 2Γ phonons. The relative intensity of the curves A, C, E is arbitrary as explained in the text.

The two-phonon contributions have been evaluated by means of equation (3.9) and the expression for the matrix elements given in section 2. The results differ for the contribution to I_{XYXY}, curve C, and to I_{XXXX}, curve D, showing that the observed two-phonon intensity will depend on the polarization of the light and the orientation of the crystal. The contribution involving both one and two-phonon processes, equation (3.8), contributes to I_{XYXY} alone and is shown in figure 4 and 5 as curve B. Since the magnitude of the two-phonon relative to the one-phonon matrix element is unknown the curves C and D may be scaled by

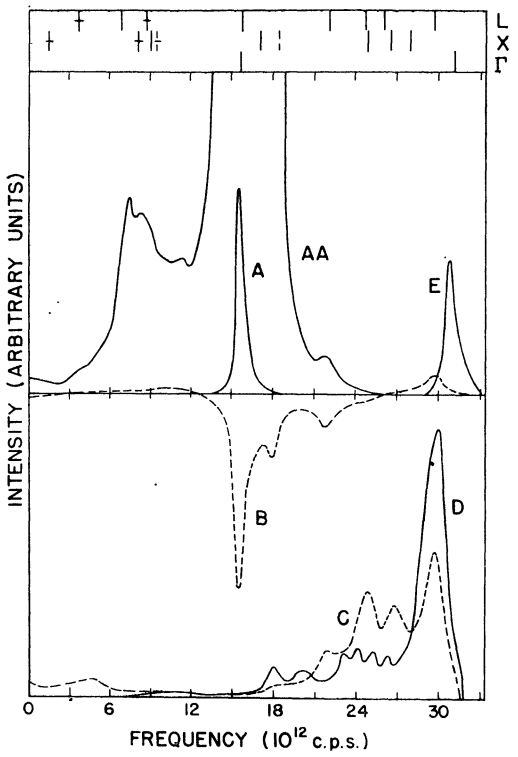

FIG. 5. — The contributions to the Raman spectra of silicon at 300 °K. The contributions are labelled similarly to these of figure 4 except the ratios of the scales for AA to A is 1/200. The critical point frequencies for Γ, X, W are also shown. Those with a horizontal bar arise from difference bands, and those dotted occur only for I_{XXXX}.

any constant K^2, while curves B are scaled by K. A further two-phonon contribution identical for both I_{XYXY} and I_{XXXX}, arises from the term involving two long wavelength optic modes and its additional contribution is shown by the curves E of figures 4 and 5. The relative intensity of this contribution is not simply related to that of the other contributions.

The detailed structure of the scattering near the one-phonon peak is of considerable interest. Figure 6 shows the detailed shape of the one-phonon contribution and it is clearly not symmetric because of the frequency dependence of $\Delta(0j, \Omega)$ and $\Gamma(0j, \Omega)$. Figure 6 also shows the contribution of the last part of expression (3.8) which is asymmetric about the one-phonon peak frequency. This contribution will act so as to shift the observed peak away from the peak in the one-phonon contribution. In the cases calculated here it appears that the size of the shift is very small, but nevertheless the detailed study of the shapes of one-phonon lines might well be rewarding.

It is also possibly of interest to point out that the size of the asymmetric term relative to the one-phonon term depends on the coefficient of the

expansion (2.1). Since the coefficients of this expansion differ for neutron and X-ray scattering and for infrared absorption the frequencies determined using these different techniques may differ, because the relative size of the asymmetric term will be different.

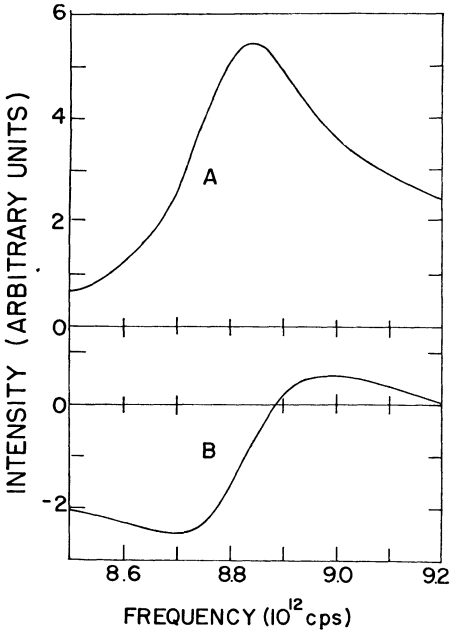

FIG. 6. — The detailed behaviour of the one-phonon contribution, A, and of the asymmetric part of B near the optic mode frequency in germanium at 300 °K.

Diamond is unfortunately the only one of the materials discussed here for which the Raman spectra has been measured. Figure 7 shows a sketch of the experimental results of Krishnan [13] compared with the spectra as calculated by the same methods as those described for germanium and silicon. Since Krishnan does not state the orientation of the specimen, the appropriate combination of the $I_{\alpha\beta\gamma\delta}$ is unknown, the calculations shown in figure 7 are for $I_{XXXX} + 3I_{XYXY}$ with a value of the parameter X chosen to give approximately a similar shape to that of the experimental results. It should be emphasized that the curve shown in figure 7 is obtained by adding parts from all the contributions A-E shown in figures 4 and 5, and far worse agreement was obtained if any of them were neglected.

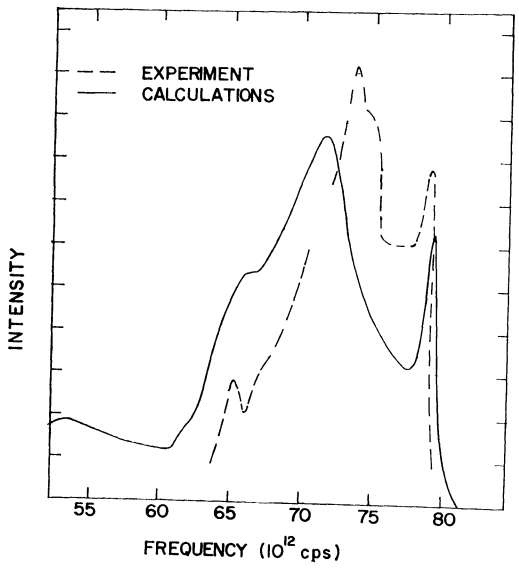

FIG. 7. — The Raman spectra of diamond as measured by Krishnan [13], dotted line, and as obtained by the present calculations, solid line.

The results show that the largest peak is displaced in the calculations by about 2 (10^{12} c. p. s.) from the largest peak in the experiment. This may possibly be due to errors in the harmonic models however, because the accuracy of the measurements of the dispersion curves on which they are based is about 3 % [14].

In view of the uncertainties in the dispersion curves, of the crystal orientation in the Raman measurements, and in the scale factor K, the agreement between the calculations and the experiment is probably as good as may be expected.

The Raman spectrum of gallium phosphide has been measured recently using a laser source, by Hobden and Russell [15]. It is of interest to compare the general shape of this spectrum with the present calculations. The spectrum of gallium phosphide shows two one-phonon peaks instead of the one for germanium and silicon. However the fine structure on the low frequency side of the one-phonon peaks is very similar in shape to that of curves AA in this region. Furthermore there are peaks near the one-phonon peaks which might result from contribution B, and at higher frequencies there are peaks which appear as though they probably arise from contributions C and D. These features seem to suggest that a combination of all these different contributions could give excellent agreement with the Raman spectra of silicon and germanium.

5. **Critical points.** — The fine structure of the Raman spectra of crystals is frequently interpreted in terms of the frequencies of the normal modes of vibration at certain special points within the Brillouin zone. Van Hove [16] showed that the one-phonon density of states plotted against frequency exhibits a discontinuity of slope, when the frequency is equal to that of a point where the gradient of the dispersion curve is zero. These points are known as critical points. This work has been extended by Johnson and Loudon [11] to give the shapes of the critical points in the two-phonon density of states function.

The interpretation of the measured Raman spectra by Bilz, Geick and Renk [9], Burstein, Johnson and Loudon [17] and Hobden and Russell [15] for example, is based on identifying the peaks and shoulders of the distributions with the frequencies of the critical points. The calculations performed in this paper are not sufficiently detailed to show the discontinuities in slope, even though they are comparable in resolution to the experimental measurements. In figure 5 the frequencies of the critical points for Γ, X, L are shown for comparison with the calculated curves for silicon. Although some of the peaks do occur at the same frequencies as the critical points, many of them occur slightly to one side of the peaks in the fine structure, or even are not readily correlated with the structure. Krishnan [13] gives a list of frequencies deduced from his measurements of which 10 are greater than a frequency of 75 (10^{12} c. p. s.), whereas the model based on the experimental dispersion curves only gives the 2Γ critical point in this frequency range. In view of these considerations it is not surprising that the dispersion curves predicted by Bilz et al. [9] and others for diamond, on the basis of critical points in the infrared and Raman spectra, show several marked discrepancies with those subsequently measured by Warren et al. [14]. Similar difficulties occur in the analysis of critical points in the two-phonon infrared spectra of crystals as described in detail by Dolling and Cowley [8].

Features of the measured spectra can clearly only be identified as critical points if the resolution of the experiments is sufficient to be able to distinguish the discontinuities in slope, to avoid the necessity of having to rely on interpretating gross features of the spectra as arising from critical points. This necessitates performing very high resolution experiments. Useful information may then be obtained about the frequencies of the critical points if the type of critical point is determined [11], and with the aid of the selection rules [8], [12]. Even under ideal conditions however, it seems unlikely that assignments can be made unambiguously in the absence of measurements of the dispersion curves.

Since very high experimental resolution is needed to establish the existence of critical points, it is necessary to examine the effects of anharmonicity on the critical points. Diagram (*a*) of figure 8 shows the ordinary two-phonon process which gives rise to the critical points in the harmonic approximation. In an anharmonic crystal both of the lines shown in diagram (*a*) can have self-energy insertions. A typical diagram of this type is (*b*). The contributions from these diagrams may be calculated by replacing the harmonic Green's functions with the dressed Green's functions in the expressions for diagram (*a*). The result is proportional to

$$\int \frac{1}{e^{\beta\hbar\omega} - 1} \rho(\mathbf{q}j, \Omega - \omega)\, \rho(-\mathbf{q}j', \omega)\, d\omega + \int \frac{1}{1 - e^{-\beta\hbar\omega}} \rho(\mathbf{q}j, \omega)\, \rho(-\mathbf{q}j', \omega - \Omega)\, d\omega, \quad (5.1)$$

where $\rho(\mathbf{q}j, \omega)$ is the spectral function of the mode $(\mathbf{q}j)$;

$$\rho(\mathbf{q}j, \omega) = \frac{4\omega(\mathbf{q}j)^2\, \Gamma(\mathbf{q}j, \omega)}{[\omega(\mathbf{q}j)^2 + 2\omega(\mathbf{q}j)\, \Delta(\mathbf{q}j, \omega) - \omega^2]^2 + 4\omega(\mathbf{q}j)\, \Gamma(\mathbf{q}j, \omega)}.$$

In general the expression (5.1) is complicated, However if we assume the modes have long lifetimes, the expression (5.1) is large when

$$\Omega = \omega(\mathbf{q}j) + 2\omega(\mathbf{q}j)\, \Delta(\mathbf{q}j, \omega(\mathbf{q}j)) \pm (\omega(\mathbf{q}j') + 2\omega(\mathbf{q}j')\, \Delta(\mathbf{q}j', \omega(\mathbf{q}j'))),$$

and the peak has a width given approximately by

$$\Gamma(\mathbf{q}j, \omega(\mathbf{q}j)) \pm \Gamma(\mathbf{q}j', \omega(\mathbf{q}j')).$$

These results show that the width of a two-phonon addition process is the sum of the lifetimes of the two independent normal modes. Since the critical point behaviour depends on the frequencies being well defined, it would clearly be impossible to observe them once the lifetimes of the normal modes became significantly large.

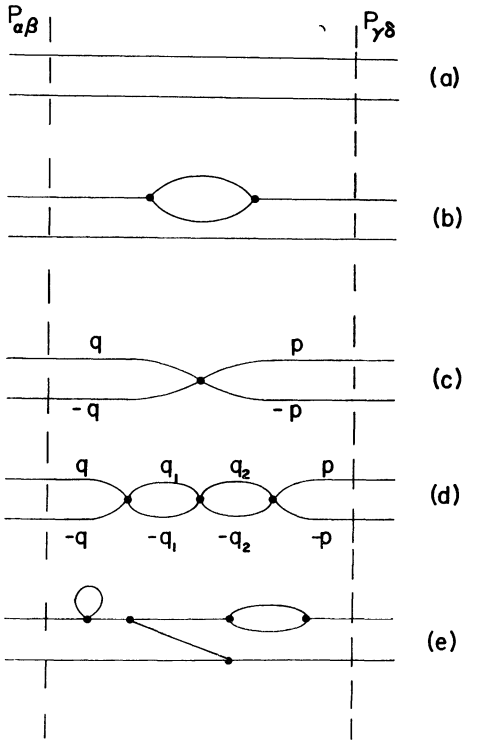

FIG. 8. — Two-phonon diagrams showing the different ways anharmonicity can enter.

Moreover not all the diagrams can be decomposed into two phonon diagrams with self-energy insertions however. Diagrams of a more complex type are shown in figure 8 (*c*) and (*d*). The contribution from diagram (*c*) is proportional to

$$\sum_{\mathbf{q}j_1j_2}\sum_{\mathbf{p}j_1'j_2'} V\begin{pmatrix}\mathbf{q} & -\mathbf{q} & \mathbf{p} & -\mathbf{p}\\ j_1 & j_2 & j_1' & j_2'\end{pmatrix}$$
$$[S(\mathbf{q}j_1 j_2, \Omega)\, R(\mathbf{p}j_1' j_2', \Omega) + R(\mathbf{q}j_1 j_2, \Omega)\, S(\mathbf{p}j_1' j_2', \Omega)], \quad (5.2)$$

where S and R are the functions defined by equations (3.4) and (3.6).

The critical point behaviour arises because of the S functions in (5.2), whereas the R functions behave smoothly. If the critical points are well defined this type of diagram will not alter the frequency or the sharpness of the critical point compared with diagram (*a*). Similar arguments can be used to show that diagram (*d*) will also leave the behaviour of the critical points unaltered. Diagram (*e*) shows another more complicated diagram including both self-energy parts and coupling between the modes.

It is of interest to compare the frequencies of the critical points with those obtained from one-phonon measurements. As remarked earlier all one-phonon measurements have an asymmetric contribution associated with them which tends to shift the frequency by amounts which vary according to the type of measurement. The two-phonon critical points do not however have any asymmetric contribution associated with them. Nevertheless this does not enable the size of the asymmetric contribution to the one-phonon results to be determined, since the asymmetric term is only considerable if the inverse lifetime of the normal modes become large. In this case the critical point is not well defined and would be difficult to identify.

6. **Summary and conclusions.** — The Raman spectra of germanium, silicon and diamond have been discussed. The models which describe the frequencies and eigenvectors of the normal modes give good agreement with the measured dispersion curves [8]. The deficiencies of the calculations probably lie in the treatment of the polarizability in terms of only a simple form of nearest neighbour interaction.

The detailed shape of the one-phonon peak has been calculated including the frequency and temperature dependent lifetime of the optic mode, and also the asymmetric term arising from the process involving both a one and two-phonon interaction. This latter term shifts the frequency of the optic mode slightly, while both effects make the peak asymmetric.

The fine structure arises from all of the different contributions : one-phonon, two-phonon and joint processes. The available experimental results [13, 15] suggest that all these contributions are needed to explain the measurements. The results also show that the fine structure depends on the polarization of the light and on the orientation of the specimen.

The frequencies of the critical points of the models are not given by the peaks in the fine structure. Critical points can only be satisfactorily determined under conditions of very good experimental resolution. Even under these conditions and with the aid of the selection rules, the author believes that their interpretation can only be made satisfactorily under extremely favourable circumstances, unless measurements of the dispersion curves have already been made by other methods.

It is hoped that these calculations will stimulate work on the Raman spectra of germanium and silicon and particularly on single crystal specimens now that laser sources are available. In particular it would be of interest to study the detailed shape of the one-phonon peak under high resolution. The fine structure appears to depend on the polarization of the light and on the orientation of the crystal. These experiments would undoubtedly show that the simple nearest neighbour type of interaction used here to describe the polarizability is inadequate, and lead to a better understanding of the processes involved in Raman scattering.

Acknowledgements. — The author is indebted to Dr. G. Dolling for his assistance and encouragement in this work. In particular he provided the shell models which gave the frequencies and eigenvectors used in these calculations.

Discussion

M. THEIMER. — Do you have some quantum mechanical estimates concerning the relative magnitude of nearest neighbours and second nearest neighbours effects on the polarizability of an atom ?

M. COWLEY. — The calculation of the matrix elements is very difficult. Second neighbour interaction is very important for the dielectric susceptibility, so it may be important for Raman scattering.

M. MARADUDIN. — In principle, every term in the expansion of the electronic polarisability in powers of the atomic displacements contributes to the intensity of the first order Raman spectrum.

Have you compared your theoretical results for diamond with those of Miss Smith ?

What is the origin of the contribution to the Raman spectrum which you have labeled E in your curves ?

M. COWLEY. — The contribution E arises from a double single phonon term in the shell model formalism (*Proc. Phys. Soc.*, 84, 281).

M. BURSTEIN. — In the case of the diamond and perhaps also in the zinc-blende structure, it would seem to me that one should expect that the matrix elements for Raman scattering would have a distinct orientation dependence, since the electron density exhibits a localization along the (111) directions which the present calculations do not take into account. In the case of NaCl type crystals, it appears, at least from the analysis of the 2nd order spectra, that the phonons at the X point make a major contribution. One might expect, in the zinc-blende and diamond structure, that the (longitudinal) phonons with atom displacements along (111) would make the major contribution. This would, for example include the longitudinal mode at the L point.

It is of interest to note that there is an interesting analogy between the second order infrared spectra of diamond type crystals and the second order Raman spectra of rocksalt type crystals. In the case of diamond type crystals which exhibit no linear moment, one must involve the second order moment mechanism for infrared absorption. The mechanical anharmonicity can not lead to absorption. In the case of rocksalt type crystals, one must involve the second order terms in the polarizability, since the first order scattering does not occur. For this structure, the anharmonic coupling makes no contribution.

M. COWLEY. — The processes involved are exactly analogous to those needed for infrared spectra.

REFERENCES

[1] BORN (M.) and HUANG (K.), Dynamical Theory of Crystal Lattices, Oxford University Press, 1954.
[2] LOUDON (R.), *Adv. in Physics*, 1964, **13**, 423.
[3] ABRIKOSOV (A. A.), GORKOV (L. P.) and DYZALOSHINSKI (I. E.), Methods of Quantum Field Theory in Statistical Physics, Prentice Hall Inc., 1963.
[4] COWLEY (R. A.), *Proc. Phys. Soc.*, 1964, **84**, 281.
[5] MARADUDIN (A. A.) and FEIN (A. E.), *Phys. Rev.*, 1962, **128**, 2589.
[6] COWLEY (R. A.), *Adv. in Physics*, 1963, **12**, 421.
[7] DOLLING (G.), Slow Neutron Scattering from Solids and Liquids, Vol. II, I. A. E. A., 1963.
[8] DOLLING (G.) and COWLEY (R. A.), To be published.
[9] BILZ (H.), GEICK (R.) and RENK (K. F.), Lattice Dynamics, p. 355, Pergamon, 1965.
[10] BIRMAN (J. L.), *Phys. Rev.*, 1962, **127**, 1093 ; *Phys. Rev.*, 1963, **131**, 1489.
[11] JOHNSON (F. A.) and LOUDON (R.), *Proc. Roy. Soc.*, 1964, **A 281**, 274.
[12] KLEINMAN (L.), *Solid State Communications*, 1965, **3**, 47.
[13] KRISHNAN (R. S.), *Proc. Ind. Acad. Sc.*, 1947 **A 26**, 399.
[14] WARREN (J. L.), WENZEL (R. G.) and YARNELL (J. L.), Inelastic Scattering of Neutrons, Vol. I, I. A. E. A., Bombay, 1964.
[15] HOBDEN (M. V.) and RUSSELL (J. P.), *Physics Letters*, 1964, **13**, 39.
[16] VAN HOVE (L.), *Phys. Rev.*, 1953, **89**, 1189.
[17] BURSTEIN (E.), JOHNSON (F. A.) and LOUDON (R.), *Phys. Rev.*, 1965, **159**, A 1239.